Linköping University Post Print

Ti$_2$Al(O,N) formation by solid state reaction between substoichiometric TiN thin films and Al$_2$O$_3$(0001) substrates

P. O. Å. Persson, Carina Höglund, Jens Birch and Lars Hultman

N.B.: When citing this work, cite the original article.

Ti$_2$Al(O,N) formation by solid-state reaction between substoichiometric TiN thin films and Al$_2$O$_3$ (0001) substrates

P.O.Å. Persson *, C. Höglund, J. Birch, L. Hultman

Thin Film Physics, Linköpings universitet, 58183 Linköping, Sweden

ABSTRACT

Titanium nitride TiN$_x$ ($0.1 \leq x \leq 1$) thin films were deposited onto Al$_2$O$_3$(0001) substrates using reactive magnetron sputtering at substrate temperatures (T_s) ranging from 800 to 1000 °C and N$_2$ partial pressures (pN$_2$) between 13.3 and 133 mPa. It is found that Al and O from the substrates diffuse into the substoichiometric TiN$_x$ films during deposition. Solid-state reactions between the film and substrate result in the formation of Ti$_2$O and Ti$_3$Al domains at low N$_2$ partial pressures, while for increasing pN$_2$, the Ti$_2$AlN MAX phase nucleates and grows together with TiN$_x$. Depositions at increasingly stoichiometric conditions result in a decreasing incorporation of substrate species into the growing film. Eventually, a stoichiometric deposition gives a stable TiN(111) || Al$_2$O$_3$(0001) structure without the incorporation of substrate species. Growth at T_s 1000 °C yields Ti$_2$AlN(0001), leading to a reduced incorporation of substrate species compared to films grown at 900 °C, which contain also Ti$_2$AlN(10$\bar{1}$3) grains. Finally, the Ti$_2$AlN domains incorporate O, likely on the N site, such that a MAX phase oxynitride Ti$_2$Al(O,N) is formed. The results were obtained by a combination of structural methods, including X-ray diffraction and (scanning) transmission electron microscopy, together with spectroscopy methods, which comprise elastic recoil detection analysis, energy dispersive X-ray spectroscopy, and electron energy loss spectroscopy.

© 2010 Elsevier B.V. All rights reserved.

1. Introduction

M$_{n+1}$AX$_n$ (MAX) phases are a family of nanolaminated ternary carbides or nitrides, where M is an early transition metal, A is a group IIIA or IVA element, and X = C or N [1]. These compounds attract interest due to their unique combination of properties [2], and several have been synthesized as bulk materials. For some time now, MAX phases are also subject of epitaxial thin film growth for which the primary deposition technique has been magnetron sputtering. A variety of M$_{n+1}$AC$_n$s deposited from either elemental or compound targets in a temperature range 800–1000 °C have been reported [3–5].

The growth of M$_{n+1}$AN$_n$ is more challenging, since N is preferably introduced into the sputtering process as a reactive gas. This is to provide for process control, albeit a small process window for the partial pressure. Until now, the only reactive sputter deposited MAX phase nitride is Ti$_2$AlN, grown from a 2Ti:Al compound target [6,7], or elemental Ti and Al targets [8,9] in a N$_2$/Ar discharge. The demanding flow control can, however, be circumvented by solid-state reactions in Ti/AlN diffusion couples. Ti$_2$AlN formation, with concurrent Ti$_3$AlN, Ti$_3$Al, and TiN, was demonstrated with this approach in polycrystalline Ti/AlN diffusion couples at annealing temperatures above 800 °C [10,11]. Topotaxial reactions in heteroepitaxial (0001) oriented Ti/AlN

diffusion couples lower the phase transformation temperature for phase-pure Ti$_2$AlN(0001) to 500 °C [12]. No reactions occur in diffusion couples of TiN/Al, independently on the amount of accessible Al or annealing temperature, and are explained by TiN and Al being thermodynamically more stable than AlN and Ti [13].

Growth of high-quality epitaxial MAX phases is promoted by a single crystal growth template. Most common is the use of MgO(111) and Al$_2$O$_3$(0001) substrates, with a nominal in plane lattice mismatch to Ti$_2$AlN(0001) of 0.33% and 10.33%, respectively. Both substrates are known to have a high thermal stability and to be chemically quite inert. Recent publications, however, have reported reaction phenomena between off-stoichiometric Ti$_2$AlN films and MgO(111) substrates at the rather low temperature 690 °C, forming a Mg$_2$(Al:Ti)O$_4$(111) spinel [14]. In addition, for substoichiometric TiC$_x$(111) films deposited onto Al$_2$O$_3$(0001), an interfacial reaction is reported to take place at 900 °C, which produces O-containing Ti$_2$AlC at the film-to-substrate interface [15]. Later it was shown that O can occupy the carbon sublattice position in Ti$_2$AlC forming a Ti$_2$Al(O,C) oxycarbide [16,17]. A first-principles investigation indicates that a solid solution of carbon and O on the carbon sublattice in Ti$_2$Al(C$_{1-x}$,O$_x$) is favorable and that amounts of O up to at least $x = 0.75$ are possible [18]. Such quaternary MAX phases provide possibilities for designing future multifunctional materials.

While no reaction in stoichiometric TiN/Al$_2$O$_3$ diffusion couples is expected due to the stability of TiN, we have found no data on the behavior of a system with N-deficient TiN$_x$ in contact with Al$_2$O$_3$. A related substrate reaction case is the formation of TiSi$_2$ at the TiN$_x$-to-Si

interface for $0.5 \leq x \leq 0.8$ [19]. Also diffusion reactions between elemental Ti and Al_2O_3 have been presented for temperatures between 425 and 1100 °C, resulting in various reaction products, like TiAl, Ti_3Al, TiO_2, Al_2TiO_5, and O-containing Ti [20–22].

Here, we present evidence of a reaction between $Al_2O_3(0001)$ substrates and reactively magnetron sputtered TiN_x ($0.1 \leq x \leq 1$) layers, forming both parallel and tilted basal plane Ti_2AlN. We also demonstrate the incorporation of O, where the O is inferred to be located on the N site, forming a quarternary $Ti_2Al(O,N)$ oxynitride MAX phase.

2. Experimental details

The deposition experiments were performed in an ultrahigh-vacuum chamber at a base pressure of 1.33×10^{-6} Pa. Magnetron sputter epitaxy (MSE), using an unbalanced type II magnetron with a 75-mm diameter Ti elemental target, was used to grow ~150-nm-thick TiN_x ($x \leq 1$) layers onto polished $10 \times 10 \times 0.5$ mm^3 $Al_2O_3(0001)$ substrates. The MSE system is described elsewhere [23]. Prior to deposition, the substrates were cleaned in ultrasonic baths of trichloroethylene, acetone, and 2-propanol and blown dry in dry N_2, followed by degassing for 1 h at the employed deposition temperature. The temperature was controlled by a thermocouple positioned behind the substrate and calibrated by pyrometry. The magnetron power was set to 200 W, and the substrate potential was set to be floating. During all depositions, the Ar partial pressure was kept at 0.666 Pa (5.0 mTorr).

Two series of depositions were performed, one with varied substrate temperature (T_s) and another with varied N_2 partial pressure (pN_2). For the temperature series, pN_2 was kept at 26.6 mPa (0.2 mTorr), while T_s was varied between 800 and 1000 °C. For the pN_2 series, T_s was kept constant at 900 °C, while pN_2 was set to 13.3, 26.6, and 39.9 mPa (0.1, 0.2, and 0.3 mTorr), with an additional 133 mPa (1.0 mTorr) sample for reference.

Elastic recoil detection analysis (ERDA), using a 40 MeV $^{127}I^{9+}$ beam at 67.5° incidence and 45° scattering angle and evaluated with the CONTES code [24], was used to follow the elemental distribution throughout the depth of the films and to check for impurities. In the analysis of the ERDA results, all elements sum up to 100 at.% at every depth position. This means that the presented atomic content in each film corresponds to the relative global amounts of a certain element at each depth position in the film.

The crystal structure was characterized by Cu $K\alpha$ X-ray diffraction (XRD) using a Philips Bragg–Brentano diffractometer.

Samples for TEM were prepared by conventional cutting, gluing, and polishing, followed by Ar ion milling using a Gatan PIPS at 5 kV for electron transparency and 1.8 kV for final polishing. Transmission electron microscopy (TEM) and (scanning) transmission electron microscopy (STEM) were performed using a FEI Tecnai TF20 UT. Simultaneous energy dispersive X-ray spectroscopy (EDX) and electron energy loss spectroscopy (EELS) elemental maps were obtained in STEM mode using EDAX Genesis 4000 and Gatan Enfina spectrometers, respectively. The EELS spectra were obtained in a diffraction coupled mode and subsequently plural-scattering deconvoluted.

3. Results

XRD data from both the pN_2 and T_s series are shown in Fig. 1. The XRD graphs in Fig. 1a show the samples grown at 900 °C and varying pN_2. Ti_2O $000l$ peaks are clearly seen at the lower partial pressures and are attenuated with increasing pN_2. These peaks are slightly shifted to higher angles. Higher order Ti_2O $000l$ peaks are also seen beyond the $\theta-2\theta$ range in Fig. 1. Additional peaks, which are suggested to be Ti_3Al 0002, and possibly a weak Ti_2AlN $10\bar{1}3$, are also present in the 13.3 mPa (0.1 mTorr) sample. At 26.6 mPa (0.2 mTorr), Ti_2AlN $000l$ and $10\bar{1}3$ peaks appear. The intensity of the $000l$ peaks increases, while the $10\bar{1}3$ peak disappears at 39.9 mPa (0.3 mTorr). Also, in the
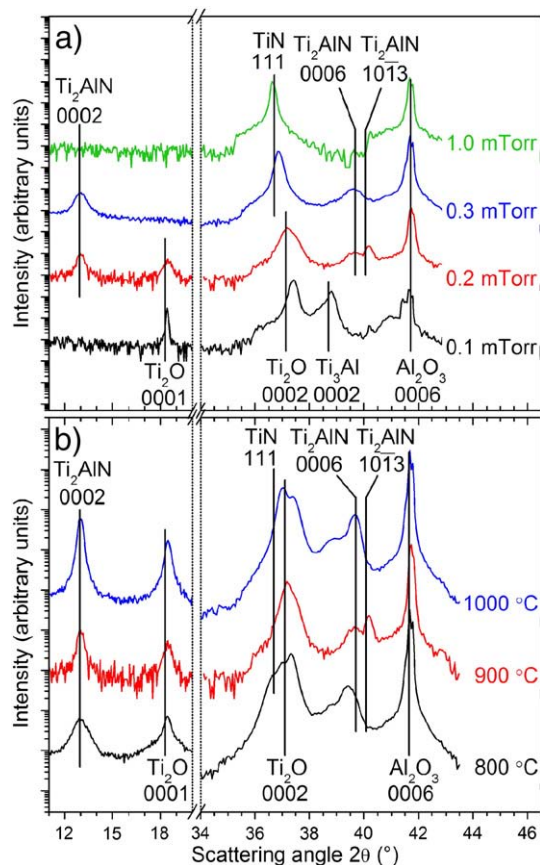

Fig. 1. XRD data recorded from a series of samples (a) grown at 900 °C with four different N_2 partial pressures and (b) grown with 26.6 mPa (0.2 mTorr) N_2 at three different temperatures.

26.6 mPa (0.2 mTorr) sample, the Ti_2O 0002 peak is allegedly two peaks, namely Ti_2O 0002 with reduced intensity and TiN_x 111. The TiN_x peak is shifted to a higher angle from the stoichiometric position but shifted continuously to lower angles with increasing pN_2 and eventually matched stoichiometric TiN 111 at $pN_2 = 133$ mPa (1.0 mTorr). At this deposition condition, no other peaks are found.

With increasing temperature and constant $pN_2 = 26.6$ mPa (0.2 mTorr), as shown in Fig. 1b, all samples contain Ti_2O, TiN_x, and Ti_2AlN peaks. The Ti_2AlN peak intensities increase with temperature and indicate $Ti_2AlN(0001)$-oriented material, except for the 900 °C sample, where also $Ti_2AlN(10\bar{1}3)$ is present. At 800 °C, the Ti_2AlN peak is also partly obstructed by a second peak. This is not positively identified but may stem from $Al_3Ti_5O_2$ or $AlTiO_2$.

Fig. 2 shows ERDA results from both pN_2 series (Fig. 2a) and T_s series (Fig. 2b), with one graph presenting the Al, Ti, N, and O elements, respectively. The Ti concentration stays nearly constant at 50–60 at.% throughout the films. With increasing pN_2 in the discharge, the N concentration increases correspondingly in the film. The presence of substrate species is clearly seen in all samples, except in the 13.3 mPa (1.0 mTorr) sample, where the concentration is below the detection limit. In particular, ~30 at. % of O is found in the 13.3 mPa (0.1 mTorr) sample, which suggests a strong diffusion of substrate species into the growing film. The 133 mPa (1.0 mTorr) film attains stoichiometric TiN and the elemental profile slopes at the film to substrate interface correspond to a sample without interdiffusion between film and substrate.

O is, in comparison, evenly distributed throughout the films, while the Al exhibits a gradually decreasing concentration from the film-to-substrate interfaces towards the film surface. This suggests that the Al containing compounds can be found near the interface while those that incorporate O may be found throughout the film.
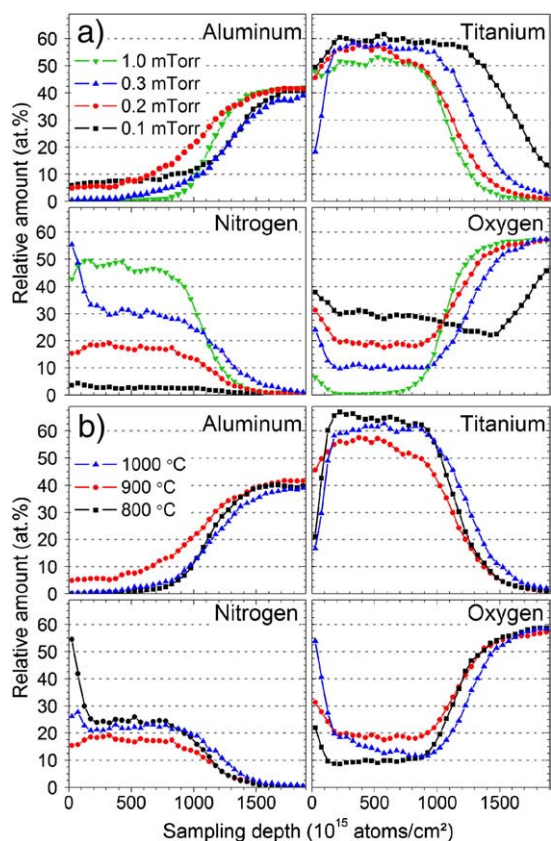
Fig. 2. ERDA data recorded from a series of samples (a) grown at 900 °C with four different N_2 partial pressures and (b) grown with 26.6 mPa (0.2 mTorr) N_2 at three different temperatures, showing the relative amount of Al, Ti, N, and O in four quadrants, respectively.

Fig. 3. TEM images with corresponding elemental maps and averaged depth profiles of the samples grown at 900 °C and different partial pressures: (a) 13.3 mPa (0.1 mTorr), (b) 26.6 mPa (0.2 mTorr), and (c) at 39.9 mPa (0.3 mTorr). In each TEM image, the film-to-substrate interface is indicated by an arrow. To the right of each TEM image, the two elemental maps show the deposited species (upper map) and substrate species (lower map). Correspondingly, the averaged depth profiles are shown next to the elemental maps for comparison. The maps and profiles are colored red (Ti) and green (N) for the deposited species and green (Al) and blue (O) for substrate species. Note the ×10 multiplier for N at 13.3 mPa (0.1 mTorr). (For interpretation of the references to color in this figure legend, the reader is referred to the web version of this article.)

For the constant partial pressure series in Fig. 2b, the compositional profiles are similar for all species, again with a more pronounced diffusion of O than Al substrate atoms. The substrate species concentration increases slightly from 800 to 900 °C, but at 1000 °C, the concentration is comparable to the 800 °C sample and lower than for 900 °C. Particularly the Al content is reduced in the film at 1000 °C, and the O content is reduced approximately by half.

The abrupt increase of O at the film surfaces, which is seen in all samples, is likely due to postgrowth indiffusion and the formation of surface oxides. Furthermore, the amount of C and H for all samples is below 0.1 at.%, which is the detection limit in ERDA.

Figs. 3 and 4 show results from the electron microscopy investigations of samples grown at constant $T_s = 900$ °C and varying pN_2, and for constant $pN_2 = 26.6$ mPa (0.2 mTorr) and varying T_s, respectively. While the TEM images provide information regarding the microstructure, the color-coded STEM-EDX maps to the right of each TEM image provide the corresponding information about the distribution of the elements. Elemental depth profiles, derived by a projection of the elemental maps, are shown to the far right to further visualize the elemental distribution.

The 13.3 mPa (0.1 mTorr) sample in Fig. 3a shows a mixture of Ti and Al near the interface to the remaining Al_2O_3, above which little Al is seen. The film exhibits a uniform distribution of a small amount of N and a substantial amount of O. Distinct boundaries are seen in the elemental maps, which correspond to the layered appearance seen in the TEM image. Judging from the elevated concentration of Al near the interface together with the XRD (c.f. Fig. 1), this initial layer consists of Ti_3Al while the thick layer reaching the surface is Ti_2O. The 26.6 mPa (0.2 mTorr) sample in Fig. 3b possesses crystallites above the interface, seen as rounded features of uniform contrast in the TEM image. At higher magnification, these crystallites can be seen to
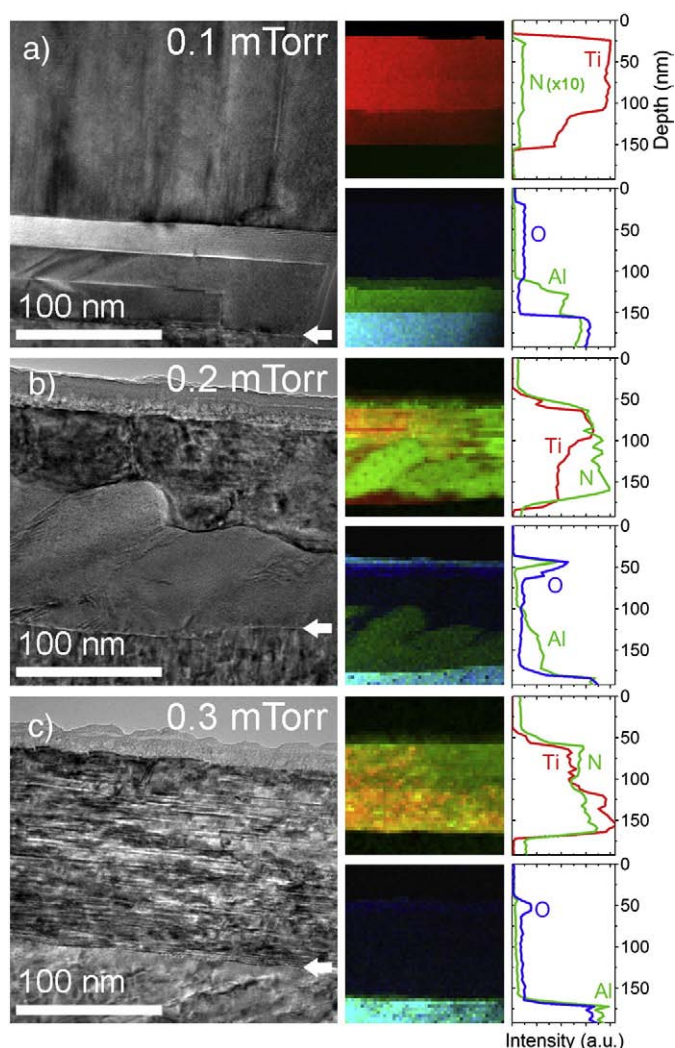
exhibit lattice fringes, which are tilted with respect to the interface (not shown). From the elemental distribution, it can be seen that these crystallites contain an elevated concentration of Al, while O displays a uniform distribution throughout the film. These crystallites are suggested to be the $Ti_2AlN(10\bar{1}3)$ MAX phase, which is found by XRD. The remaining material, closer to the surface, exhibits a cubic structure, as seen by high-magnification TEM (not shown), which is oriented with the close packed 111 planes parallel to the interface, corresponding to the TiN_x peak seen by XRD in Fig. 1. This structure contains a large number of stacking faults with small amounts of (0001) MAX phase intercalated, as seen by high-magnification TEM (not shown). Finally, the 39.9 mPa (0.3 mTorr) sample in Fig. 3c displays a continuous film with a significant amount of stacking faults, separating (0001) MAX phase layers, primarily located near the interface or otherwise embedded in the (111) cubic material throughout the film. Corresponding elemental maps suggest a uniform distribution of all elements with the resolution of the measurement.
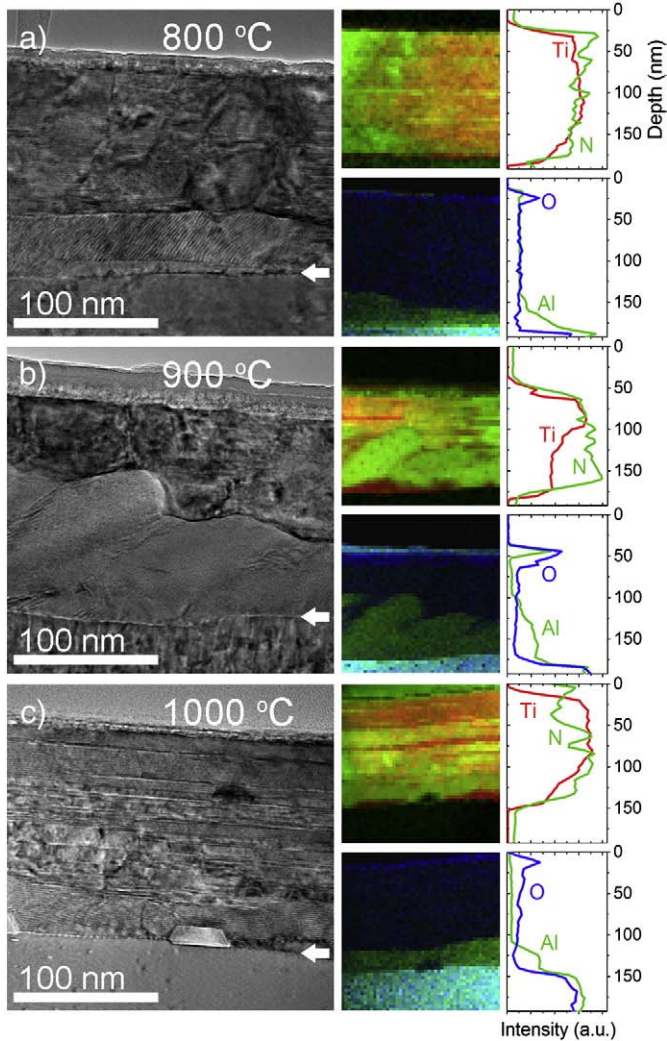
Fig. 4. TEM images with corresponding elemental maps and averaged depth profiles of the samples grown with 26.6 mPa (0.2 mTorr) N_2 at different temperatures: (a) 800 ºC, (b) 900 ºC, and (c) 1000 ºC. In each TEM image, the film-to-substrate interface is indicated by an arrow. To the right of each TEM image, the two elemental maps show the deposited species (upper map) and substrate species (lower map). Correspondingly, the averaged depth profiles are shown next to the elemental maps for comparison. The maps and profiles are colored red (Ti) and green (N) for the deposited species and green (Al) and blue (O) for substrate species. Note that the maps in (a) are slightly shifted to the right compared to the TEM image.

For the 800 ºC sample in Fig. 4a, the film contains crystallites at the interface, which exhibit fringes that are tilted with respect to the interface. This is presumably a MAX phase layer, since it is seen to incorporate the Al in the film, although this tilted orientation was not found in the XRD data in Fig. 1. Above this phase and reaching to the film surface, the material in the TEM image exhibits weak fringes, which are oriented parallel to the substrate surface, and is suggested to be a mixture of the $TiN_x(111)$ and $Ti_2O(000l)$ material found by XRD. The Ti and N distribution is even in this film with some tendency for N to segregate laterally. While there is an apparent preference for Al to be associated with the alleged MAX phase crystallites near the interface, O is as previously uniformly distributed. The 900 ºC sample is identical to Fig. 3b but is shown here for comparison. At 1000 ºC, as shown in Fig. 4c, the film exhibits a large amount of stacking faults, separating cubic $TiN_x(111)$-like layers from $Ti_2AlN(0001)$ domains, which were identified by high-magnification TEM (see Fig. 5 below). Near the interface to the substrate, there is a well-ordered layer of $Ti_2AlN(0001)$ MAX phase. Investigating the elemental distribution in Fig. 4c), Al is again found primarily in the MAX phase located at the
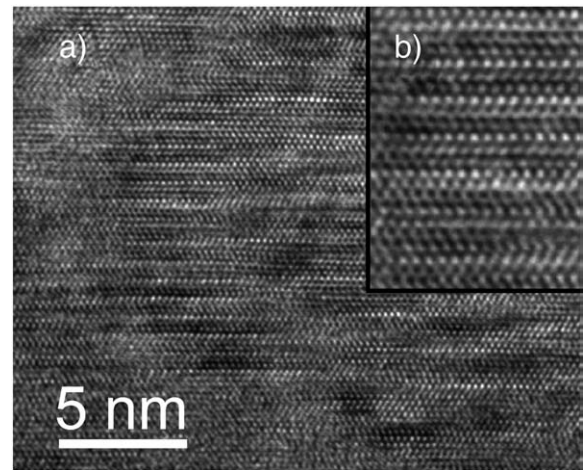

Fig. 5. High-resolution TEM images of the MAX phase layer of the film deposited at 1000 °C obtained from near the interface to the substrate and deposit from the 1000 ºC sample, in (a) overview and (b) higher magnification.

interface, which indicates a segregation of Al into TiN_x, and a transformation of TiN_x into Ti_2AlN through a solid state reaction. The location of Al in the structures corresponds well to the ERDA results, where for the 800 and 1000 ºC samples, Al is segregated to MAX phase material above the film-to-substrate interface. At 900 ºC, Al is segregated to $Ti_2AlN(10\bar{1}3)$ MAX phase crystallites, which extend further from the interface, compared to the other two samples. For the deposited species, a distinct sectioned appearance can be seen for N. Correspondingly, the O map displays an inverse distribution. These sections may indicate a separation between Ti_2O and TiN_x which are identified by XRD. The faceted feature found at the interface in Fig. 4c is suggested to contain O, since the feature appears as a void in all elemental maps except the O map. As for the ERDA measurements, an apparent increase in the O content is seen at the surface of the maps in Figs. 3 and 4.

The most well-ordered and continuous Ti_2AlN layer was found in the 1000 ºC sample. A high-resolution TEM image and diffraction coupled EEL spectrum from this layer is shown in Figs. 5 and 6, respectively. The high-resolution image shows a well-ordered (0001)-oriented structure and the inset in Fig. 5b, at slightly higher magnification, reveals in more detail the zig–zag structure of the hexagonal phase, with the A element located in the mirror planes. Apart from the low-loss region, the plural scattering deconvoluted core-loss region from 395 to 590 eV is shown in the EEL spectrum, as it contains the N–K, $Ti–L_{2,3}$ and the O–K edges at ~400, ~450, and ~530 eV, respectively. Consequently, the apparent Ti_2AlN MAX phase also binds O.
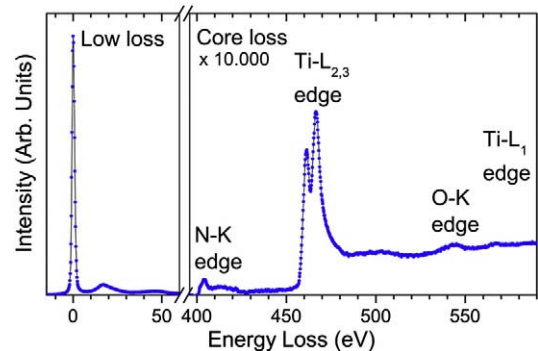

Fig. 6. Diffraction coupled EEL spectrum including the low loss spectrum and the N–K, Ti–L, and O–K edges from the MAX phase layer shown in Fig. 5.

4. Discussion

The above results show that during deposition of substoichiometric TiN_x films on $Al_2O_3(0001)$ substrates, the deposited material reacts with the substrate. This leads to the uptake of substrate species Al and O and nucleation of various phases in the films. Depositions with an increasing pN_2 at $T_s = 900$ °C result in an increasing amount of N in the films. With increasing N content, the incorporation of substrate species decreases correspondingly, suggesting a declining substrate reaction. At stoichiometric TiN deposition conditions, there is no reaction with the substrate and no substrate species are found in the film. The distribution of elements was shown from compositional analyses by ERDA, EDX, and EELS. The two former reveal that O is evenly distributed in nearly all films, while Al is primarily located near the film-to-substrate interface.

The compounds that form at low pN_2 are Ti_2O and Ti_3Al, as seen by XRD, and indicate how the O and Al species are incorporated. When incorporating more N in the film through a higher pN_2, the reaction with the substrate decreases such that the Ti_2O is no longer nucleated and the reduced amount of O is incorporated in other phases of the film. At 39.9 mPa (0.3 mTorr) pN_2, only TiN_x and Ti_2AlN are formed. The compositional measurements reveal a uniform distribution of O in this film, which thus must be incorporated in these two phases. The TiN 111 peak is found to shift to higher angles with decreasing intensity at lower pN_2. This may be explained by either a large amount of N vacancies [25,26] or O incorporation on the N site, as TiN is isomorphous to TiO [27]. The Ti_2O $000l$ peaks are also found to shift towards higher 2θ angles, which may occur due to similar arguments.

The Al incorporation in the film is driven by the formation of Ti_2AlN, which nucleates in both (0001) and $(10\bar{1}3)$ orientations. With increasing N content, the Ti_2AlN peak intensity increases in XRD, and assumes a (0001) texture, which also is seen in the TEM and HREM images. At $pN_2 = 133$ mPa (1.0 mTorr), the nucleation of a stoichiometric TiN film impedes any substrate-related reactions. A corresponding reaction was reported for substoichiometric TiC_x deposition on Al_2O_3 substrates, such that increased substoichiometry sets off the reaction [17]. In either case, the reaction is driven by thermodynamics.

Depositions at constant pN_2 and $T_s = 800$ ºC and 900 ºC result in the nucleation of the (0001) MAX phase near the substrate interface that grows into domains, which also exhibit $(10\bar{1}3)$ orientation at 900 ºC, as is seen by XRD and high-magnification TEM (not shown). It is also found that the domains contain substrate material according to the elemental maps in Fig. 4a and b. The ERDA depth profiles also corroborate the elemental distribution, showing that for these samples, the Al distribution extends further from the interface with increasing temperature in accordance with a diffusion process. However, at the highest temperature 1000 ºC, the concentration of both Al and O decreases throughout the film. This film, however, no longer contains $Ti_2AlN(10\bar{1}3)$ and only Ti_2AlN (0001) remains. Diffusion of the A element in MAX phases has been found to occur preferably along the basal plane, e.g., in Ti_3SiC_2 [28]. Increased diffusion of the A element (Al) towards the film surface from the substrate is enabled through growth of $(10\bar{1}3)$-oriented crystals. For the material, which is nucleated in a (0001) orientation, the diffusion of substrate material must occur perpendicular to the basal planes, which slows down the vertical diffusion process, given that our layers are epitaxial and contain effectively no grain boundaries. Upward diffusion could be enabled by threading dislocations in the MAX layer. Consequently, one way to reduce the amount of substrate material in the films is to grow low-defect-density (0001)-oriented material. Another way to remove the reaction is to deposit stoichiometric film material.

The deposited thickness of the films was found to vary, with the thickest films resulting from the lowest pN_2 deposition. This thickness variation may be caused by the fact that a higher pN_2 leads to an increasingly nitrided Ti sputter target accompanied by a lower sputtering rate. This phenomenon is not expected to contribute significantly to the observed variation in thickness. A stronger contribution to the thickness variation probably stem from the incorporation of substrate material into the film, which is apparently stronger at lower pN_2, and effectively contributes to the thickness of the grown film.

Finally, the incorporation of O in the MAX phase was investigated. In the 1000 ºC sample, the MAX phase layer near the interface is of high quality and was chosen for this experiment. According to the elemental maps, this layer consists only of the Ti_2AlN. Here, the elements Ti and N were detected by EELS, while Al was found in the MAX phase using EDX. The core loss spectrum in Fig. 6 also connects O to Ti_2AlN, proving structural incorporation of O. O was recently found to be incorporated substitutionally on the C site in Ti_2AlC, forming a $Ti_2Al(O,C)$ phase [17]. To determine on which lattice site the O resides, fine structure calculations should be performed along with better signal-to-noise EELS measurements. However, in analogy with the similar Ti_2AlC MAX phase, it is likely that the O resides on the N site and forms a $Ti_2Al(O,N)$ oxynitride MAX phase. This would mean that the O forms a local TiO structure in the MX slabs.

5. Conclusions

Substoichiometric TiN_x $(x<1)$ thin films deposited by reactive magnetron sputtering in a mixed N_2/Ar discharge at 800–1000 °C react with $Al_2O_3(0001)$ substrates. For nitrogen-depleted conditions, the films consist of Ti_2O and Ti_3Al. Increasing the N content leads to the formation of TiN_x and Ti_2AlN. It is only at stoichiometric deposition conditions of TiN that no substrate species are found in the films. The Ti_2AlN phase can form in both the (0001) and $(10\bar{1}3)$ orientations. The $Ti_2AlN(0001)$ layers reduce interdiffusion of substrate elements by limiting the diffusion to the basal planes. Finally, O released in the film-to-substrate reaction becomes incorporated in Ti_2AlN, presumably by substitution for N. Thus, a MAX phase oxynitride $Ti_2Al(O,N)$ is formed.

References

[1] V.H. Nowotny, Prog. Solid State Chem. 5 (1971) 27.
[2] M.W. Barsoum, T. El-Raghy, Am. Sci. 89 (2001) 334.
[3] J.-P. Palmquist, U. Jansson, T. Seppänen, P.O.Å. Persson, J. Birch, L. Hultman, P. Isberg, Appl. Phys. Lett. 81 (2002) 835.
[4] T. Seppänen, J.-P. Palmquist, P.O.Å. Persson, J. Emmerlich, J. Molina, J. Birch, U. Jansson, P. Isberg, L. Hultman, in: J. Keränen, K. Sillanpää (Eds.), 53rd Annual Meeting of the Scandinavian Society for Electron Microscopy, Tampere University, Tampere, 2002, p. 142.
[5] P. Eklund, M. Beckers, U. Jansson, H. Högberg, L. Hultman, Thin Solid Films 518 (2010) 1851.
[6] T. Joelsson, A. Hörling, J. Birch, L. Hultman, Appl. Phys. Lett. 86 (2005) 111913.
[7] T. Joelsson, A. Flink, J. Birch, L. Hultman, J. Appl. Phys. 102 (2007) 074918.
[8] M. Beckers, N. Schell, R.M.S. Martins, A. Mücklich, W. Möller, Appl. Phys. Lett. 89 (2006) 074101.
[9] P.O.Å. Persson, S. Kodambaka, I. Petrov, L. Hultman, Acta Mater. 55 (2007) 4401.
[10] Y. Imanaka, M.R. Notis, J. Am. Ceram. Soc. 82 (1999) 1547.
[11] C.-H. Chiu, C.C. Lin, J. Am. Ceram. Soc. 89 (2006) 1409.
[12] C. Höglund, M. Beckers, N. Schell, J.v. Borany, J. Birch, L. Hultman, Appl. Phys. Lett. 90 (2007) 174106.
[13] C. Höglund, Ph.D. Thesis Linköping Studies in Science and Technology No. 1314, 2010.
[14] M. Beckers, N. Schell, R.M.S. Martins, A. Mücklich, W. Möller, L. Hultman, J. Appl. Phys. 102 (2007) 074916.
[15] P.O.Å. Persson, J. Rosén, D.R. McKenzie, M.M.M. Bilek, C. Höglund, J. Appl. Phys. 103 (2008) 066102.
[16] J. Rosen, P.O.Å. Persson, M. Ionescu, A. Kondyurin, D.R. McKenzie, M.M.M. Bilek, Appl. Phys. Lett. 92 (2008) 064102.
[17] P.O.Å. Persson, J. Rosen, D.R. McKenzie, M.M.M. Bilek, Phys. Rev. B 80 (2009) 092102.
[18] N. Dahlqvist, B. Alling, I.A. Abrikosov, J. Rosén, Phys. Rev. B 81 (2010) 024111.
[19] N. Fujimura, T. Ito, Appl. Surf. Sci. 41 (42) (1989) 272.
[20] B.-J. Lee, Acta Mater. 10 (1997) 3993.
[21] A. Zalar, B. Baretzky, F. Dettenwanger, M. Rühle, P. Panjan, Surf. Interface Anal. 26 (1998) 861.
[22] O.M. Ndwandwe, M.S. Mpungose, S. Afr. J. Sci. 102 (2006) 244.
[23] J. Birch, S. Tungasmita, V. Darakchieva, Trivandrum (2002) 421.
[24] M.S. Janson, CONTES Conversion of Time–Energy Spectra—A Program for ERDA Data Analysis, Internal Report, Uppsala University, 2004.
[25] L.E. Toth, Transition Metal Carbides and Nitrides, Academic Press NY, 1971.
[26] C.-S. Shin, D. Gall, N. Hellgren, J. Patscheider, I. Petrov, J.E. Greene, J. Appl. Phys. 93 (2003) 6025.
[27] H.O. Pierson, Handbook of Refractory Carbides and Nitrides, William Andrew Publishing/Noyes, 1996.
[28] J. Emmerlich, D. Music, P. Eklund, O. Willhelmsson, U. Jansson, J.M. Schneider, H. Högberg, L. Hultman, Acta Mater. 55 (2007) 1479.